Room temperature weak ferromagnetism in $Sn_{1-x}Mn_xSe_2$ 2D films grown by molecular beam epitaxy

Sining Dong,[1] Xinyu Liu,[1] Xiang Li,[1] Vasily Kanzyuba,[1] Taehee Yoo,[1,2] Sergei Rouvimov,[3,4] Suresh Vishwanath,[3,5] Huili G. Xing,[3,5,6] Debdeep Jena,[3,5,6] Margaret Dobrowolska,[1] and Jacek K. Furdyna[1]

[1]*Department of Physics, University of Notre Dame, Notre Dame, Indiana 46556, USA*
[2]*Department of Physics, Korea University, Seoul 136-701, South Korea*
[3]*Department of Electrical Engineering, University of Notre Dame, Notre Dame, Indiana 46556, USA*
[4]*Notre Dame Integrated Imaging Facility, University of Notre Dame, Notre Dame, Indiana 46556, USA*
[5]*School of Electrical and Computer Engineering, Cornell University, Ithaca, New York 14853, USA*
[6]*Department of Materials Science and Engineering, Cornell University, Ithaca, New York 14853, USA*

(Received 30 November 2015; accepted 8 February 2016; published online 24 February 2016)

We discuss growth and magnetic properties of high-quality two dimensional (2D) $Sn_{1-x}Mn_xSe_2$ films. Thin films of this 2D ternary alloy with a wide range of Mn concentrations were successfully grown by molecular beam epitaxy. Mn concentrations up to $x \approx 0.60$ were achieved without destroying the crystal structure of the parent $SnSe_2$ 2D system. Most important, the specimens show clear weak ferromagnetic behavior above room temperature, which should be of interest for 2D spintronic applications. [http://dx.doi.org/10.1063/1.4942637]

Two-dimensional (2D) crystals have been receiving considerable attention due to their unique electronic and optical properties that open new research routes for basic research and hold promise of novel device applications.[1–5] The new 2D semiconductor $SnSe_2$ is an important member of this class of materials, having structural properties similar to the well-studied 2D transition-metal dichalcogenide (2D-TMD) crystal family (e.g., MoS_2, $MoSe_2$, and WTe_2), involving a hexagonal structure with two-dimensional chalcogen-metal-chalcogen layers bonded by van der Waals forces (see inset in Fig. 2). Similar to 2D-TMD systems, $SnSe_2$ exhibits very attractive optoelectronic properties.[6,7] Additionally, it also has a very high bulk electron affinity and can thus form a near-broken gap alignment with other 2D-TMDs[8,9] that holds special promise for interband tunneling devices.

Based on the pioneering work on graphene which paved the way to the new field of 2D spintronics,[10] it appears especially important to obtain 2D materials with ferromagnetic properties, which can then be exploited in the next generation of spintronic devices. In this context, the introduction of magnetic dopants into the 2D lattice of this family of materials constitutes a promising method toward this goal, by creating new functionalities for spintronic applications in a 2D environment.[11] However, very little work on ferromagnetic 2D materials has so far been reported. With this in mind, in the present work, we describe an exploratory investigation on the growth and characterization of ternary-alloy $Sn_{1-x}Mn_xSe_2$ thin film, where (as will be shown) the presence of Mn results in clear magnetic properties that survive to and above room temperature. Importantly, we find that even rather large concentrations of Mn (up to $x \approx 0.6$) do not destroy the basic 2D crystal structure of the parent compound $SnSe_2$. We feel therefore that these findings may open the path toward obtaining ferromagnetic 2D films at nanoscale thicknesses.

The $Sn_{1-x}Mn_xSe_2$ films were grown on GaAs (111)B substrates by a Riber-32 molecular beam epitaxy (MBE) system with a reflection high-energy electron diffraction (RHEED) monitor. The

(111)B substrate orientation is chosen because of its compatibility with the hexagonal structure of the $SnSe_2$ structure. The epi-ready substrates were directly loaded into the MBE chamber (vacuum level is $\sim 10^{-10}$ Torr), were first deoxidized at 580 °C and then annealed at around 600 °C for 20 min in Se flux ($\sim 1.5 \times 10^{-6}$ Torr), and were then cooled down to 150 °C in preparation for the growth of $Sn_{1-x}Mn_xSe_2$. During the cooling process, the GaAs substrate was exposed to a Se flux in order to form monolayer GaSe buffer at the substrate surface and to further smooth out the surface when the substrate was above 300 °C. During the growth process, the $SnSe_2$ phase forms naturally when the Sn/Se flux ratio is less than 1:100. A series of $Sn_{1-x}Mn_xSe_2$ samples with different Mn concentrations were grown by using different Mn effusion cell temperatures.

The $Sn_{1-x}Mn_xSe_2$ samples used for structural measurements had a thickness of ~40 nm, and for magnetic measurements had a thickness of ~80 nm, with a 7 nm $SnSe_2$ capping layer and a final 3 nm aluminum layer to prevent oxidation after the samples are exposed to the atmosphere. X-ray diffraction (XRD) spectra were measured using a Bruker D8 X-ray diffractometer. The cross-sectional scanning transmission electron microscope (STEM) images of the samples were carried out using an FEI Titan 80-300 microscope with STEM specimens prepared using an FEI-Helios dual beam focused ion beam (FIB) workstation. The energy dispersive X-ray (EDX) spectra were obtained using an FEI-Magellan 400 field-emission scanning electron microscope (FESEM) equipped with a Bruker energy dispersive X-ray spectrometer. Finally, the magnetic properties of the samples were studied using a superconducting quantum interference device (SQUID) magnetometer (Quantum Design MPMS XL).

Figure 1(a) shows the RHEED pattern of a GaAs (111)B substrate after vacuum annealing and prior to the $Sn_{1-x}Mn_xSe_2$ growth. Figures 1(b)-1(d) present RHEED patterns of, respectively, $SnSe_2$ and $Sn_{1-x}Mn_xSe_2$ films after a 40 min growth, indicating that the films are flat good-quality single

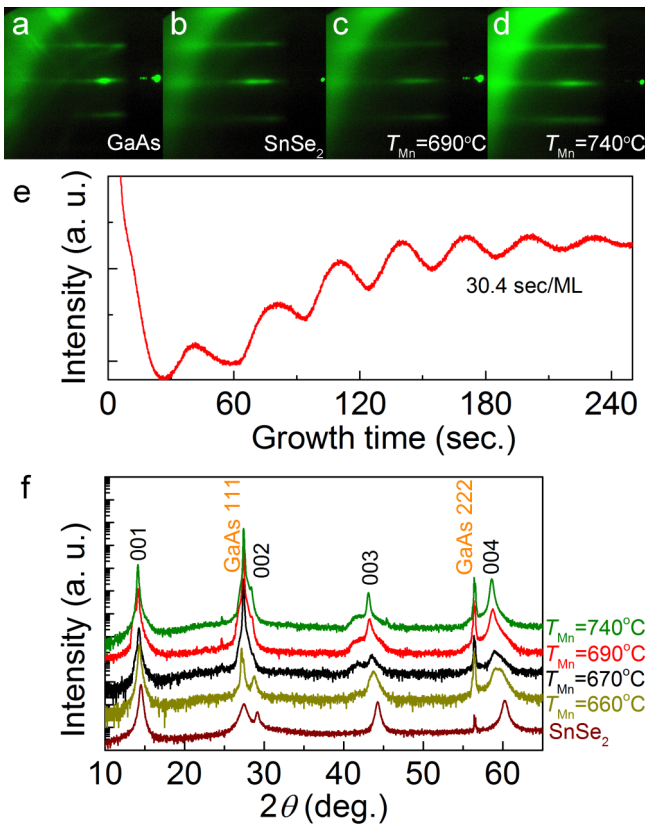

FIG. 1. RHEED patterns observed on the GaAs (111) substrate (a), and during the growth of $SnSe_2$ (b) and of $Sn_{1-x}Mn_xSe_2$ films with different Mn effusion cell temperatures (T_{Mn}) ((c) and (d)). (e) RHEED oscillation profile for the sample growing at $T_{Mn} = 690$ °C. (f) XRD spectra of $Sn_{1-x}Mn_xSe_2$ films grown with different values of T_{Mn}.

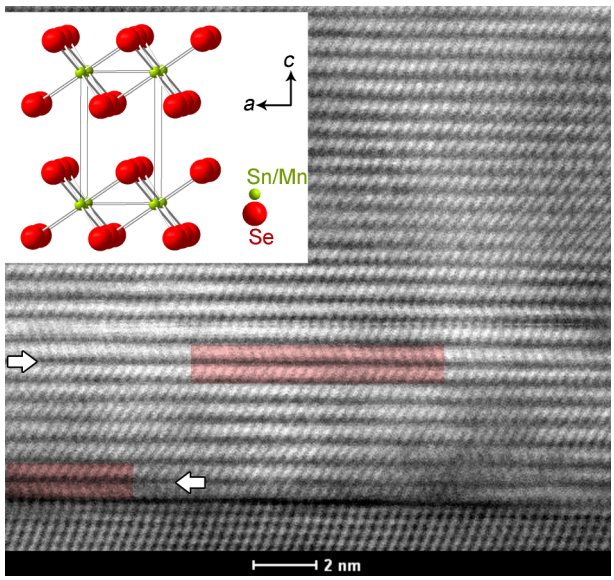

FIG. 2. Cross-sectional STEM image of the $Sn_{1-x}Mn_xSe_2$ film grown with $T_{Mn} = 670\,°C$ along the [010] zone axis of $SnSe_2$. The inset shows the structural schematic of the $SnSe_2$ crystal. Note the mirror stacking layers marked by arrows and highlighted in red.

crystals. Additionally, it can be inferred from the RHEED results that the in-plane lattice parameter of $Sn_{1-x}Mn_xSe_2$ is slightly smaller than that of the GaAs (111) surface. Finally, Fig. 1(e) shows a RHEED oscillation profile of the $Sn_{1-x}Mn_xSe_2$ sample for the T_{Mn} = 690 °C growth, its clear oscillations indicating layer-by-layer growth with a growth rate of about 30.4 s/monolayer (ML). The growth rate increases slightly with increasing Mn effusion cell temperature (by about 1 s/ML per 10 °C, data not shown). The XRD patterns for the $Sn_{1-x}Mn_xSe_2$ films are shown in Fig. 1(f). The samples show only (00*l*) peaks of the $SnSe_2$ structure, illustrating excellent *c*-axis-oriented epitaxial growth. A weak shoulder is seen near the (003) peak of the $SnSe_2$-structure, which we ascribe to the presence of possible nano-inclusions in the MnSe phase.[12] This peak is seen to disappear in samples grown at lower values of T_{Mn}, suggesting that traces of this phase form at high Mn concentrations. Except for that, all $Sn_{1-x}Mn_xSe_2$ specimens grown under conditions described above show excellent $SnSe_2$-structure, which appears not to be affected by the presence on Mn.

Figure 2(a) shows the cross-sectional STEM image of the $Sn_{1-x}Mn_xSe_2$ film grown with T_{Mn} = 670 °C. Although the in-plane lattice mismatch between $Sn_{1-x}Mn_xSe_2$ and GaAs is quite small (about 4.6% as calculated from GaAs and $SnSe_2$ crystal parameters), an inspection of the interface region between the two materials indicates that the first few layers of the $Sn_{1-x}Mn_xSe_2$ film are already relaxed, without indications of significant lattice matching at the interface. This is an important feature of heterostructures involving van der Waals epitaxy,[13] indicating that this mechanism governs the growth of the present $Sn_{1-x}Mn_xSe_2$/GaAs system as well. It is also notable that mirror stacking between layers and within the layers occurs in this growth (see stacking between the first and second, and between 7th and 8th layers counting from the interface, marked by arrows and highlighted in red). Analysis of our TEM and XRD results indicates that the Mn ions in our films substitutionally replace a fraction of the Sn ions. Quantitatively, the Mn concentration in our $Sn_{1-x}Mn_xSe_2$ films was obtained from the analysis of EDX spectra shown in Fig. 3. The resulting Mn concentrations for different growths are listed Table I. Figure 3(b) shows the Mn concentration as a function of Mn effusion cell temperature T_{Mn}. One can see that the Mn concentration increases linearly from about 42% to 66% as T_{Mn} increases from 670 °C to 760 °C. It is important that as already noted, the parent $SnSe_2$-type structure remains essentially unchanged even after half of the Sn sites become occupied by Mn ions. It is interesting, however, that the Se concentration appears to decrease somewhat in samples grown at the highest Mn effusion cell temperatures. This may be related to the emergence of the MnSe phase in samples grown at higher values of T_{Mn}, as seen in the XRD data. We note parenthetically that

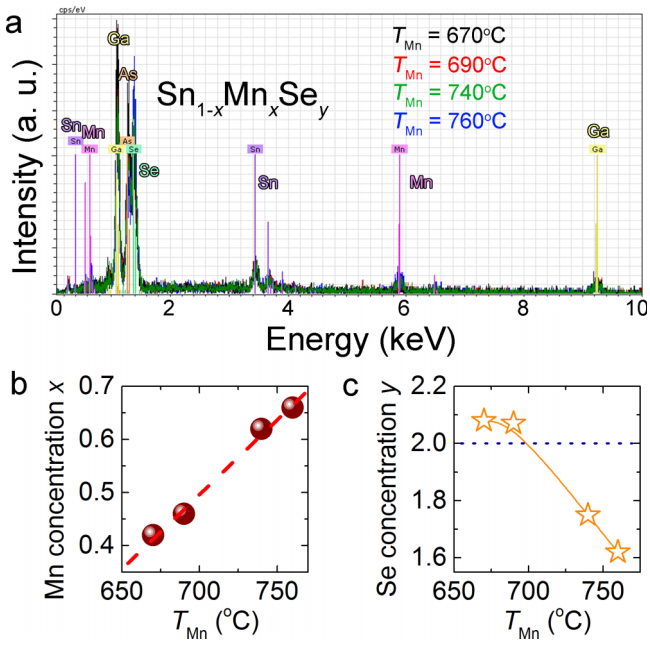

FIG. 3. (a) EDX spectra of $Sn_{1-x}Mn_xSe_2$ films grown at different Mn effusion cell temperatures. ((b) and (c)) Mn effusion cell temperature dependences of the Mn concentration (b) and of the Se concentration (c).

formation of MnSe in MBE growth at high Mn flux is consistent with in our early studies for the magnetic II–VI chalcogenide systems with high Mn concentrations and may thus explain the reduced overall concentration of Se that we observe as the Mn concentration increases.[14]

Figure 4 shows the out-of-plane magnetization of the $Sn_{1-x}Mn_xSe_2$ films as a function of temperature, measured by SQUID in a magnetic field of 200 Oe. It can be seen that the magnetization is relatively weak for all the samples. Interestingly, the temperature dependence of magnetization data in Fig. 4 shows that the samples grown at T_{Mn} = 740 °C and T_{Mn} = 760 °C (i.e., with highest values of x) have an additional magnetic transition at 120 K. While the mechanism for this is not understood, it is possible that the observed feature may arise from the formation of α-MnSe inclusions, since that material has a Néel temperature of 122 K.[15] α-MnSe is an antiferromagnet, but at nanoscale its inclusions may have significant magnetic moments due to the presence of uncompensated spins,[16,17] which would account for the observed increase of magnetization below 120 K. We clearly see from Fig. 4, however, that the magnetic order exhibited by the $Sn_{1-x}Mn_xSe_2$ alloy itself survives in all samples up to at least 400 K.

Figure 5 shows out-of-plane hysteresis loops for our $Sn_{1-x}Mn_xSe_2$ films measured at 300 K and 10 K. Weak but clear ferromagnetic-like signals are reproducibly observed for all specimens. We ascribe the observed behavior to the magnetically uncompensated Mn moments responding to the applied field in the presence of an antiferromagnetically coupled majority of Mn ions. All samples show larger saturation magnetizations and larger coercive fields at 10 K than at room temperature. By a rough calculation, the moment per Mn atom in a field of 5 kOe in the sample grown at T_{Mn} = 670 °C is

TABLE I. Composition of $Sn_{1-x}Mn_xSe_y$ films from EDX analysis.

T_{Mn} (°C)	Composition
670	$Sn_{0.58}Mn_{0.42}Se_{2.08}$
690	$Sn_{0.54}Mn_{0.46}Se_{2.07}$
740	$Sn_{0.38}Mn_{0.62}Se_{1.75}$
760	$Sn_{0.34}Mn_{0.66}Se_{1.62}$

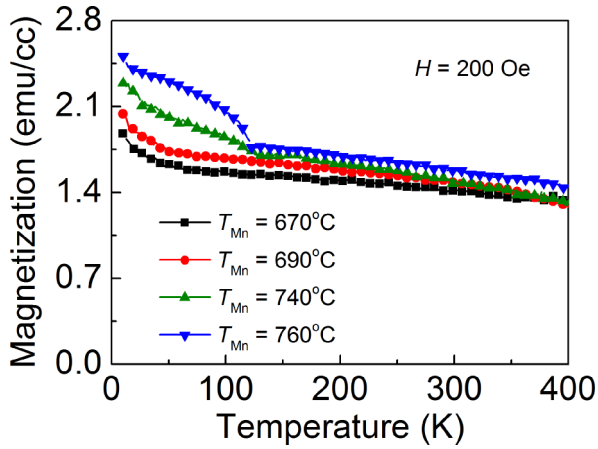

FIG. 4. Temperature dependence of out-of-plane magnetization of $Sn_{1-x}Mn_xSe_2$ films grown at different Mn effusion cell temperatures.

about 0.06 μ_B and that in grown at T_{Mn} = 760 °C is about 0.09 μ_B at 300 K, respectively. This suggests that most of the Mn ions in the $Sn_{1-x}Mn_xSe_2$ system are coupled antiferromagnetically, so that the net moment results only from those Mn ions that are not fully compensated by the surrounding Mn ions. In particular, we note that with the increasing value of x, the total magnetization of the $Sn_{1-x}Mn_xSe_2$

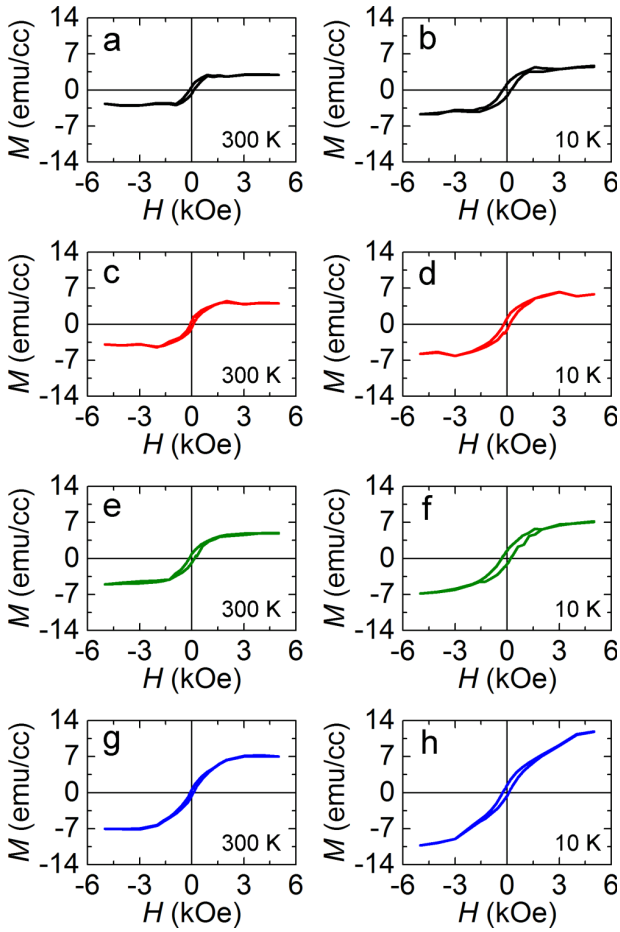

FIG. 5. Out-of-plane hysteresis loops of $Sn_{1-x}Mn_xSe_2$ films grown at Mn effusion cell temperatures of 670 °C ((a) and (b)), 690 °C ((c) and (d)), 740 °C ((e) and (f)), and 760 °C ((g) and (h)) measured at 300 K and 10 K.

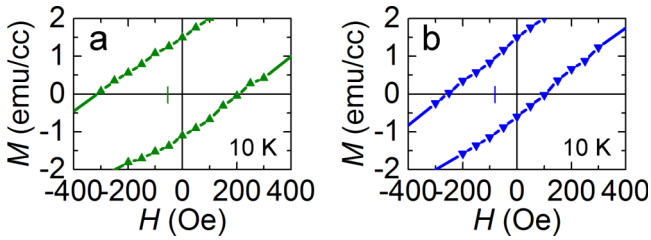

FIG. 6. Zoomed-in low-field view of out-of-plane hysteresis loops for $Sn_{1-x}Mn_xSe_2$ films grown at Mn effusion cell temperatures of 740 °C (a) and 760 °C (b) measured at 10 K after cooling in a 5 kOe field, showing the presence of exchange bias.

films slightly increases, indicating that the concentration of magnetically uncompensated Mn ions increases with x. Additionally, the slight increase of the magnetic moment per Mn ion as total Mn concentration increases suggests the distribution of uncompensated Mn spin is random throughout the entire $Sn_{1-x}Mn_xSe_2$ film. One should note here that, although nano-inclusions of the α-MnSe phase mentioned above (as well as possible inclusions of $MnSe_2$ or zinc-blende MnSe) could indeed form during the MBE growth of $Sn_{1-x}Mn_xSe_2$, the magnetic ordering temperature of all three of these phases occurs well below room temperature.[18,19] Thus the room temperature weak ferromagnetism observed in our samples can only originate from the $Sn_{1-x}Mn_xSe_2$ alloy itself.

Careful inspection of the hysteresis loops of the samples grown with T_{Mn} = 740 °C and T_{Mn} = 760 °C also exhibits exchange bias shifts after cooling in a field of +5 kOe, as shown in Fig. 6. Specifically, hysteresis loop centers of these samples shift in a direction opposite to the applied cooling field. The observed shift can be described as $H_{EB} = (H_1 + H_2)/2$, where H_{EB} is the exchange bias field, and H_1 and H_2 are the observed left and right coercive fields, respectively.[20] This provides H_{EB} of 53 Oe and 76 Oe, respectively, for the samples grown at 740 °C and 760 °C, suggesting that exchange bias increases with increasing Mn concentration. In contrast, no such shift can be detected in the 10 K hysteresis loops for the samples with lower Mn concentrations (i.e., those grown with T_{Mn} = 670 °C and T_{Mn} = 690 °C). This suggests that the origin of the observed exchange bias is related to the origin of the magnetic transition shown in Fig. 4 at 120 K for specimens with the higher values of Mn concentration. If the magnetic contribution to the magnetization observed in $Sn_{1-x}Mn_xSe_2$ samples grown with higher Mn flux near 120 K can be attributed to α-MnSe nano-inclusions, as discussed earlier, the exchange bias phenomenon could then result from exchange coupling between the weakly ferromagnetic $Sn_{1-x}Mn_xSe_2$ matrix and such antiferromagnetic MnSe nano-inclusions.[21] However, many details remain to be further investigated in this system before drawing more definitive conclusions.

In summary, good quality $Sn_{1-x}Mn_xSe_2$ films with relatively high Mn concentrations have been successfully grown by MBE on GaAs (111)B substrates. Our results indicated that the Mn content of the films can be readily tuned by Mn effusion cell temperature without affecting the parent $SnSe_2$ crystal structure. All samples show weak net ferromagnetic-like signals at room temperature due to a small fraction of magnetically uncompensated Mn magnetic moments, in the presence of an antiferromagnetic background associated with the majority Mn population. The slight increase of the magnetic moment per Mn ion observed as the total Mn concentration increases suggests that the distribution of uncompensated Mn spins is random throughout the films. Apart from their basic interest, these findings also suggest a path toward fabricating ferromagnetic 2D materials for spin-based device applications.

This work was supported by NSF Grant Nos. DMR14-00432 and DMR14-33490. S. N. Dong was also supported by the NNSF of China (Contract No. 51302257). T. Yoo was supported by the National Research Foundation of Korea under Grant No. 2013R1A1A2004505.

[1] S. Z. Butler, S. M. Hollen, L. Cao, Y. Cui, J. A. Gupta, H. R. Gutierrez, T. F. Heinz, S. S. Hong, J. Huang, and A. F. Ismach, ACS Nano **7**, 2898 (2013).
[2] L. Britnell, R. Ribeiro, A. Eckmann, R. Jalil, B. Belle, A. Mishchenko, Y.-J. Kim, R. Gorbachev, T. Georgiou, and S. Morozov, Science **340**, 1311 (2013).
[3] Y. Zhang, T. Oka, R. Suzuki, J. Ye, and Y. Iwasa, Science **344**, 725 (2014).

[4] F. Withers, O. Del Pozo-Zamudio, A. Mishchenko, A. Rooney, A. Gholinia, K. Watanabe, T. Taniguchi, S. Haigh, A. Geim, A. Tartakovskii, and K. S. Novoselov, Nat. Mater. **14**, 301 (2015).
[5] K. Kang, S. Xie, L. Huang, Y. Han, P. Y. Huang, K. F. Mak, C.-J. Kim, D. Muller, and J. Park, Nature **520**, 656 (2015).
[6] D. Martínez-Escobar, M. Ramachandran, A. Sánchez-Juárez, and J. S. N. Rios, Thin Solid Films **535**, 390 (2013).
[7] X. Zhou, L. Gan, W. Tian, Q. Zhang, S. Jin, H. Li, Y. Bando, D. Golberg, and T. Zhai, Adv. Mater. **27**, 8035 (2015).
[8] R. Schlaf, O. Lang, C. Pettenkofer, and W. Jaegermann, J. Appl. Phys. **85**, 2732 (1999).
[9] Y. Su, M. A. Ebrish, E. J. Olson, and S. J. Koester, Appl. Phys. Lett. **103**, 263104 (2013).
[10] S. Roche, B. Beschoten, J.-C. Charlier, M. Chshiev, S. P. Dash, B. Dlubak, J. Fabian, A. Fert, F. Guinea, and I. Grigorieva, 2D Mater. **2**, 030202 (2015).
[11] K. Zhang, S. Feng, J. Wang, A. Azcatl, N. Lu, R. Addou, N. Wang, C. Zhou, J. Lerach, and V. Bojan, Nano Lett. **15**, 6586 (2015).
[12] M. E. Schlesinger, Phase equilib **19**, 588 (1998).
[13] A. Geim and I. Grigorieva, Nature **499**, 419 (2013).
[14] N. Samarth, H. Luo, J. Furdyna, S. Qadri, Y. Lee, R. Alonso, E. Suh, A. Ramdas, and N. Otsuka, Surf. Sci. **228**, 226 (1990).
[15] R. Pollard, V. McCann, and J. Ward, J. Phys. C: Solid State Phys. **16**, 345 (1983).
[16] S. Dong, Y. Yao, Y. Hou, Y. Liu, Y. Tang, and X. Li, Nanotechnology **22**, 385701 (2011).
[17] K. V. Manukyan, Y.-S. Chen, S. Rouvimov, P. Li, X. Li, S. Dong, X. Liu, J. K. Furdyna, A. Orlov, and G. H. Bernstein, J. Phys. Chem. C **118**, 16264 (2014).
[18] Q. Peng, Y. Dong, Z. Deng, H. Kou, S. Gao, and Y. Li, J. Phys. Chem. B **106**, 9261 (2002).
[19] N. Samarth, P. Kłosowski, H. Luo, T. Giebułtowicz, J. Furdyna, J. Rhyne, B. Larson, and N. Otsuka, Phys. Rev. B **44**, 4701 (1991).
[20] S. Dong, D. Zhang, Y. Liu, S. Yang, T. Jiang, Y. Yin, and X. Li, Nanoscale **6**, 14766 (2014).
[21] J. Nogués, J. Sort, V. Langlais, V. Skumryev, S. Surinach, J. Munoz, and M. Baró, Phys. Rep. **422**, 65 (2005).